DOI: 10.1002/ejic.200900188

Two New Supramolecular Architectures of Singly Phenoxo-Bridged Copper(II) and Doubly Phenoxo-Bridged Manganese(II) Complexes Derived from an Unusual ONOO Donor Hydrazone Ligand: Syntheses, Structural Variations, Cryomagnetic, DFT, and EPR Studies

Aurkie Ray,[a] Corrado Rizzoli,[b] Guillaume Pilet,[c] Cédric Desplanches,[d] Eugenio Garribba,[e] Eva Rentschler,[f] and Samiran Mitra*[a]

Keywords: Supramolecular chemistry / Structure elucidation / Density functional calculations / N,O ligands / Hydrogen bonds / Bridging ligands

Two new coordination complexes {[(**L**)Cu_2(μ-**L**)(NO_3)-(CH_3OH)$_{0.3}$(H_2O)$_{0.7}$]·NO_3}[Cu(**L**)(NO_3)(CH_3OH)] (**1**) and [Mn_2(μ-**L**)$_2$(H_2O)(μ$_1$-N_3)$_2$(CH_3OH)] (**2**) derived from (*E*)-*N*′-(2-hydroxy-3-methoxybenzylidene)acetohydrazide [**LH**] have been synthesized. The new potentially tetradentate ONOO donor hydrazone ligand [**LH**] has shown considerable metal ion selective phenoxo bridging in **1** and **2**. It has coordinated copper(II) ions in its tridentate as well as in tetradentate fashion whereas for manganese(II) ions it solely showed its tetradentate character. In **1** the two adjacent pentacoordinate copper(II) centers are connected by a rare single phenoxo linkage of the hydrazone ligand whereas **2** is a doubly phenoxo-bridged heptacoordinated manganese(II) dinuclear species. The 3D supramolecular networks of **1** and **2** have resulted from extensive H-bonding interactions in the respective complexes. Structural variations observed for **1** and **2** have been described by performing single-crystal X-ray analysis. The ligand and the complexes are characterized by elemental analyses, IR, UV/Vis and ^{1}H NMR spectroscopy. Cryomagnetic investigations, DFT studies and EPR analysis, of **1** and **2** have also been studied in detail.

Introduction

Supramolecular architectures of the coordination complexes through hydrazone ligand-based hydrogen-bonding interactions are very rare and not yet explored.[1] Earlier many authors and our research group reported several coordination complexes derived by aroylhydrazones for their pharmacological activity and magnetic properties[2a] but such complexes were devoid of any hydrogen-bonding interactions that could generate supramolecular architectures with intriguing structures.[2] Recently Chattopadhyay and his group have shown how the supramolecular architecture of manganese(II) aroyl hydrazone complexes can be controlled by slight modification of the substituents attached to the ligand framework.[3] The self-assembly of multimetallic assemblies held together by intermolecular forces (hydrogen bonds, van der Waals forces etc.) is greatly dependent on the metal ions.[4] Metal ions can read the information coded in the organic ligands according to their coordination algorithm[5] and thereby give rise to metal–organic ligand complex species that are simultaneously assembled via complementary interligand hydrogen bonding forming supramolecular multimetallic assemblies. Metal–organic frameworks containing channels or pores with various sizes and shapes have attracted much attention because of their potential applications in catalysis, separation and gas sorption and storage.[6–8] The interactions of hydrogen bonds play vital roles for molecular recognition in a wide variety of biological systems and have also been applied in the synthesis of molecular magnetic materials.[9] In order to generate hydrogen-bonding interactions in hydrazone metal complexes we synthesized a new NNO donor hydrazone ligand derived from an aliphatic hydrazide (acetic hydrazide) and reported two new coordination complexes with copper(II)

[a] Department of Chemistry, Jadavpur University, Raja S. C., Mullick Road, Kolkata – 700 032, India
Fax: +91-033-2414-6414
E-mail: smitra_2002@yahoo.com
[b] Universitá degli Studi di Parma, Dip.di Chimica GIAF, Viale G.P. Usberti 17/A, 43100 Parma, Italy
[c] Groupe de Cristallographie et Ingénierie Moléculaire, Laboratoire des Multimatériaux et Interfaces UMR 5615 CNRS – Université Claude Bernard Lyon 1, Bât. Jules Raulin, 43 bd. du 11 Novembre 1918, 69622 Villeurbanne, Cedex, France
[d] ICMCB, CNRS, Université Bordeaux 1, 87, Avenue du Dr. A. Schweitzer, 33608 Pessac Cedex, France
[e] Department of Chemistry, University of Sassari, Via Vienna 2, 07100 Sassari, Italy
[f] Johannes Gutenberg University of Mainz, Institute of Inorganic and Analytical Chemistry, Duesbergweg 10–14, 55128 Mainz
Supporting information for this article is available on the WWW under http://dx.doi.org/10.1002/ejic.200900188.

and cobalt(III); in both the complexes the H-bonding interactions generated 1D chain and 2D grid-like polymeric structures.[10]

To further explore the coordination behavior of the hydrazone ligand derived from acetic hydrazide with different metal ions, we synthesized a new tetradentate ONOO donor hydrazone ligand [**LH**] as the 1:1 condensation product of acetic hydrazide and vanillin (the procedure of synthesis of **LH** and the two different coordination modes are shown in Scheme 1) and have reported two new complexes **1** and **2**.

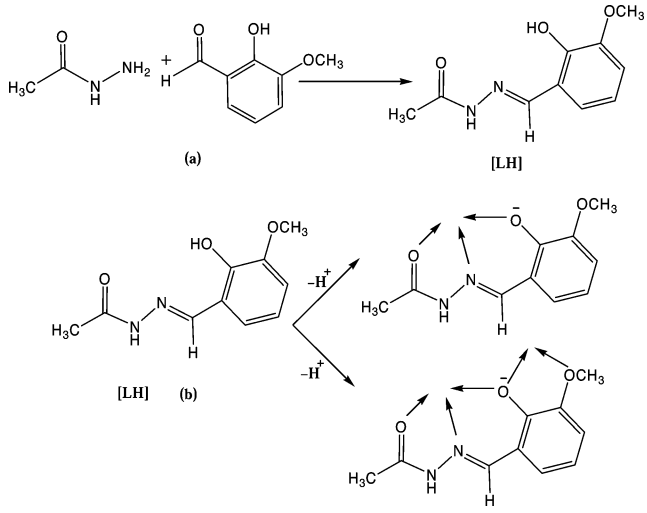

Scheme 1. (a) Synthesis of **LH**, (b) two different coordination modes of the potentially tetradentate ONOO donor hydrazone ligand.

Although the new hydrazone ligand [**LH**] has shown metal ion-selective coordination behavior with copper(II) and manganese(II) ions, the ligand-based N–H and C–H hydrogen-bonding interactions with NO_3^-, N_3^-, coordinated and uncoordinated solvent molecules have led to the formation of two new intriguing metal–organic frameworks containing channels and zig-zag layer structures in the respective complexes. Earlier in 2003 we reported the first singly phenoxo-bridged copper(II) dinuclear complexes[11] derived from an amino-containing NNOO donor Schiff base ligand and in this paper we report another new singly phenoxo-bridged pentacoordinate copper(II) complex (**1**) derived from an ONOO donor hydrazone ligand. Unlike the earlier complexes[11] the asymmetric unit of **1** comprises of a singly phenoxo-bridged copper(II) dinuclear cationic unit associated with a copper(II) neutral mononuclear unit.

Contrary to **1**, **2** is a doubly phenoxo-bridged heptacoordinated manganese(II) dinuclear species resulting from the metal ion selective coordination of the ONOO donor hydrazone ligand [**LH**]. Another contrasting aspect which distinguishes the manganese(II) complex from the copper(II) complex is that **2** contains two terminally coordinating azido ligands. The authors have deliberately used sodium azide during the synthesis of **2** as unlike the five-coordinated copper(II) complex (**1**), the manganese(II) complex generally prefers a higher coordination number (six or seven) and in the absence of azido ligands the authors are unable to obtain single crystals of **2** with **LH**. Earlier Blondin and Aukauloo reported several doubly phenoxo-bridged hexacoordinate manganese(II) dinuclear species derived from a pentadentate NNNNO donor Schiff base ligand[12] but heptacoordinated doubly phenoxo-bridged manganese(II) dinuclear complexes derived from a tetradentate ONOO donor hydrazone ligand still remain unexplored. From a literature survey we found that in 2007 an analogous ONOO donor aroylhydrazone: *N*′-(2-hydroxy-3-methoxybenzylidene)benzohydrazide [**L′H**] (obtained by 1:1 condensation of benzhydrazide and vanillin) was used to synthesize a mononuclear manganese(II) complex but the single crystal structure is not yet known.[13] As an extension of the work we have used **L′H** to synthesize a novel tetra(μ_3-phenoxo)-bridged copper(II) complex containing a Cu_4O_4 cubane core.[14] By replacing the phenyl moiety in **L′H** with a methyl moiety we have obtained the new tetradentate hydrazone ligand [**LH**]. It is interesting to note that the two analogous ONOO donor hydrazone ligands [**L′H** and **LH**] have shown significant variation in their coordination behavior with copper(II) ions, as a consequence of which two entirely different copper(II) coordination complexes of different nuclearity have resulted.

The new hydrazone ligand [**LH**] and its complexes **1** and **2** have been characterized from elemental analyses, IR, UV/Vis and ^{1}H NMR spectroscopy. Single crystal X-ray diffraction study of **1** and **2** confirms the selective coordination behavior of **LH** with copper(II) and manganese(II) ions and also help us to identify the different H-bonding interactions responsible for generating 3D supramolecular architectures in the respective complexes. Cryomagnetic investigations and DFT studies of **1** and **2** have been studied in order to explain the observed magnetic coupling operating in the complexes. The authors have performed detailed EPR analyses for **1** and **2** both in solid state and in different solvent systems ($CHCl_3$/toluene, DMF, or CH_3CN) in order to show how the complex evolves from solid-state to solution and how it is highly dependent on the solvent used.

Results and Discussion

Synthesis of the New Hydrazone Ligand [LH]

Our group is the first to report (*E*)-*N*′-(2-hydroxy-3-methoxybenzylidene)acetohydrazide [**LH**] derived from an aliphatic hydrazide. The tetradentate ONOO donor hydrazone ligand was prepared by the 1:1 condensation of acetichydrazide with vanillin (synthesis of **LH** is depicted in Scheme 1). In 2008 we reported two new metal hydrazone complexes derived from (*E*)-*N*′-[(pyridin-2-yl)methylene] acetohydrazide ligand[10] and to further explore the coordination chemistry of metal hydrazone complexes derived from an aliphatic hydrazide we synthesized the ligand [**LH**]. The ligand was isolated in virtually quantitative yield and satisfactorily characterized by elemental analysis and IR, mass and ^{1}H NMR spectroscopy.

Crystal Structure Descriptions

{[(L)Cu_2(μ-L)(NO_3)(CH_3OH)$_{0.3}$(H_2O)$_{0.7}$]·NO_3}[Cu(L)(NO_3)(CH_3OH)] (1)

The asymmetric unit of **1** contains two distinct copper(II) units (Figure 1), a dinuclear cationic unit [(**L**)Cu_2(μ-**L**)(NO_3)(CH_3OH)$_{0.3}$(H_2O)$_{0.7}$]$^+$ (**L** = 2-acetylhydrazonomethyl-5-methoxyphenolato), whose charge is counterbalanced by a nitrate anion, and a mononuclear neutral unit [Cu(**L**)(NO_3)(CH_3OH)].

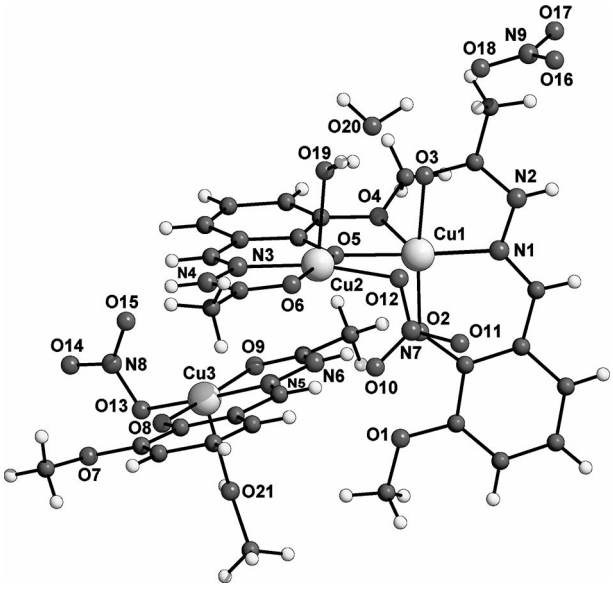

Figure 1. Asymmetric unit of **1** containing a dinuclear copper(II) cationic unit and a neutral copper(II) mononuclear unit.

The structural aspects of the dinuclear cationic unit of **1** has been compared to that of the earlier reported singly phenoxo-bridged dinuclear copper(II) complexes [Cu_2(L)$_2$(SCN)(H_2O)](ClO_4) (**A**), [Cu_2(L)$_2$(N_3)(H_2O)](ClO_4) (**B**), and [Cu_2(L)$_2$(NCO)(H_2O)](ClO_4) (**C**).[11] It should be noted that compounds **B** and **C** are isostructural to that of **A** and all three complexes contain geometrically different square-pyramidal copper(II) centers, with NNNOO and NNOOO donor sets. Unlike **A**, **B**, and **C** the copper(II) centers (Cu1 and Cu2) residing in the dinuclear cationic unit of **1** (Figure 2), display a geometrically equivalent distorted square-pyramidal geometry with NOOOO donor sets. The O2, O3, N1 donor atoms of a deprotonated ligand [**L**]$^-$ fulfill three basal positions around Cu1, while the remaining basal and apical sites are completed by the O5 and O4 atoms of the second [**L**]$^-$ ligand. Atom O5 acts as a bridge between the metal centers (Cu1 and Cu2), also occupying a basal position around Cu2. The coordination around Cu2 is completed by the O6, N3 atoms of the second ligand and the O10 atom of a nitrate anion at the base, and by the O19 oxygen atom of a statistically distributed water/methanol molecule at the apex. In **1** the singly phenoxo-bridged Cu1···Cu2 separation is 3.20 Å which is shorter than the Cu···Cu separation found in **A**, **B**, and **C** [3.291(2) Å]. Moreover, the Cu1–O5–Cu2 angle in **1** is 109.96(15)° which is close to that of the similar singly phenoxo-bridged complexes[11] [in **A**, **B**, and **C** the Cu1–O5–Cu2 angles are 111.5(1), 109.3(2), and 109.6(1)°, respectively]. The basal CuO_3N cores in the dinuclear cationic unit are nearly orthogonal, the dihedral angle they form being 80.15(12)°.

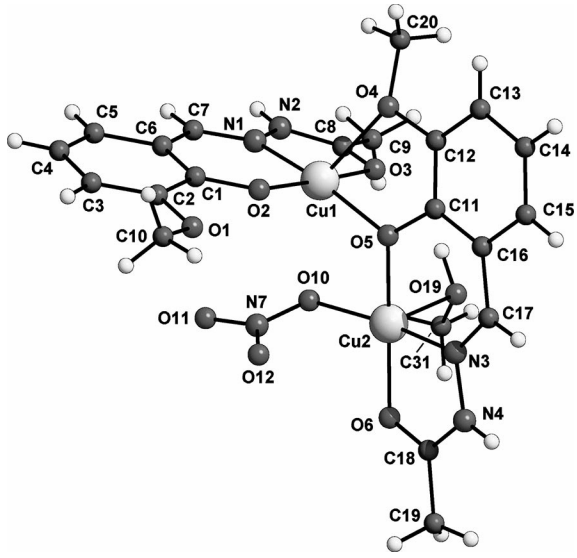

Figure 2. The singly phenoxo-briged copper(II) dinuclear cationic unit of **1**.

In the neutral complex molecule (Figure 3), coordination around the Cu3 metal is similar to that observed for the Cu2 atom, with the keto O, imine N, phenoxo O, atoms of a hydrazone ligand [**L**]$^-$ and one oxygen atom of a nitrate anion occupying the basal positions of a distorted square-pyramid, and with the oxygen atom of a methanol molecule at the apex. The Cu–N (mean value 1.92 Å) and Cu–O bond lengths involving the oxygen atoms at the basal planes (mean value 1.95 Å) fall in a rather narrow range (Table 1). Of the three independent monoanionic [**L**]$^-$ ligands protonated at N2, N4, and N6 respectively, one displays a tetradentate coordination mode (containing N4) whereas the other two (containing N2, N6) display a tridentate coordination mode. The protonation at N2, N4, and N6 of the three independent monoanionic [**L**]$^-$ ligands suggests that the ligand has not undergone enolization and has coordinated the copper(II) centers in its keto form.

The tridentate coordination mode of [**L**]$^-$ results in the formation of five- and six-membered metallacycles. The negative charge is localized at the oxygen atoms of the six-membered chelating rings, as indicated by the double-bond character of the C8–O3, C18–O6 bond lengths (mean value 1.25 Å), which are remarkably shorter than the C–O bonds (C1–O2, C11–O5, C21–O8; mean value 1.32 Å) involving the oxygen atoms of the five-membered rings. As a consequence, the values of the N1–C7, N3–C17, and N5–C27 bonds (mean value 1.28 Å) within the five-membered chelating rings are consistent with a significant double-bond character. All five- and six-membered chelating rings are roughly planar [maximum displacement 0.128(3) Å for

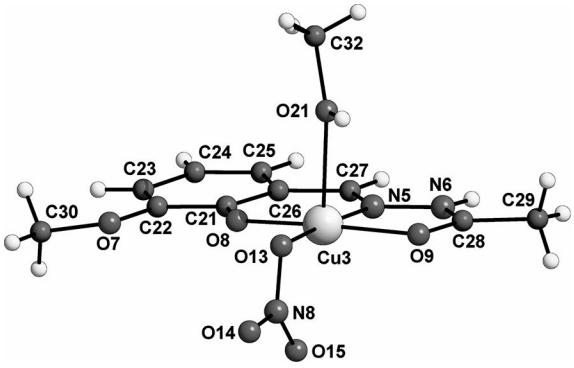

Figure 3. The neutral copper(II) mononuclear unit of **1**.

Table 1. Selected bond lengths [Å] and bond angles [°] for **1**.

Bond lengths		Bond lengths	
Cu1–O2	1.916(4)	Cu2–O19	2.246(4)
Cu1–O3	1.980(4)	Cu2–N3	1.929(4)
Cu1–O4	2.313(4)	Cu3–O8	1.907(3)
Cu1–O5	1.983(3)	Cu3–O9	1.995(4)
Cu1–N1	1.927(4)	Cu3–O13	1.955(4)
Cu2–O5	1.935(3)	Cu3–O21	2.450(5)
Cu2–O6	1.952(4)	Cu3–N5	1.914(4)
Cu2–O10	1.972(3)	–	–
Bond angles		**Bond angles**	
O2–Cu1–O3	173.95(14)	C31–O19–Cu2	113.3(13)
O2–Cu1–O5	93.45(14)	C7–N1–Cu1	128.6(4)
O2–Cu1–O4	95.35(15)	N2–N1–Cu1	111.3(3)
O2–Cu1–N1	92.56(16)	O6–Cu2–O19	94.61(16)
O3–Cu1–O4	88.47(15)	O6–Cu2–N3	81.40(17)
O3–Cu1–O5	92.10(14)	O10–Cu2–O19	93.09(16)
O3–Cu1–N1	81.56(16)	O10–Cu2–N3	169.19(18)
O4–Cu1–N1	115.41(15)	O19–Cu2–N3	97.67(16)
O5–Cu1–O4	74.07(13)	O8–Cu3–O9	171.75(15)
O5–Cu1–N1	168.23(15)	O8–Cu3–O13	93.58(17)
O5–Cu2–O6	169.99(15)	O8–Cu3–O21	100.78(16)
C12–O4–Cu1	110.3(3)	O8–Cu3–N5	92.17(17)
C20–O4–Cu1	126.4(4)	O9–Cu3–O13	93.48(16)
C11–O5–Cu2	125.9(3)	O9–Cu3–O21	84.70(16)
C11–O5–Cu1	122.2(3)	O9–Cu3–N5	80.72(16)
Cu2–O5–Cu1	109.96(15)	O13–Cu3–O21	79.55(19)
C18–O6–Cu2	113.0(3)	O13–Cu3–N5	174.17(19)
C21–O8–Cu3	127.0(3)	O21–Cu3–N5	100.3(2)
C28–O9–Cu3	112.1(3)	C1–O2–Cu1	126.7(3)
N7–O10–Cu2	113.7(3)	C8–O3–Cu1	112.0(3)
N8–O13–Cu3	111.0(4)	C17–N3–Cu2	129.2(4)
O5–Cu2–O10	88.85(14)	N4–N3–Cu2	111.0(3)
O5–Cu2–O19	93.37(15)	C27–N5–Cu3	129.6(4)
O5–Cu2–N3	91.56(16)	N6–N5–Cu3	111.9(3)
O6–Cu2–O10	96.74(16)	–	–

atom O5] and, within each ligand, are slightly folded about the Cu–N bonds, the dihedral angles formed by the least-square planes through them being 3.01(13), 4.83(9), and 3.30(9)° for the hydrazone ligands coordinated to Cu1, Cu2, and Cu3, respectively. The crystal structure is stabilized by an extended three-dimensional network of C–H···O, N–H···O, O–H···O intra- and intermolecular hydrogen-bonding interactions (Table 2, Figure 4).

Table 2. Hydrogen bond parameters of **1**.

D–H···A	*d*(D–H) [Å]	*d*(H···A) [Å]	*d*(D···A) [Å]	∠ (DHA)°
O19–H19D···O3	0.93	2.14	3.016(4)	157.5
O19–H19E···O20	0.93	1.86	2.774(10)	165.5
O20–H20D···O8	0.96	1.94	2.897(10)	173.8
N6–H6N···O1	0.86	2.37	2.785(6)	110.4
N6–H6N···O2	0.86	2.00	2.855(7)	176.5
C25–H25···O12	0.93	2.35	3.206(9)	152.7
C27–H27···O12	0.93	2.51	3.336(10)	148.3
O19–H19D···O17^{i}	0.93	2.57	2.955(7)	105.3
C9–H9A···O20^{i}	0.96	2.55	3.349(9)	141.0
O20–H20E···O15^{ii}	0.93	2.15	3.077(8)	173.9
O21–H21···O9^{iii}	0.87	2.02	2.890(7)	172.9
C29–H29C···O13^{iii}	0.96	2.52	3.328(9)	142.2
N2–H2N···O8^{iv}	0.86	2.01	2.845(7)	164.3
N2–H2N···O13^{iv}	0.86	2.51	3.031(5)	119.5
N4–H4N···O16^{v}	0.86	2.31	3.092(8)	152.1
N4–H4N···O17^{v}	0.86	2.18	2.968(8)	152.9
C17–H17···O17^{v}	0.93	2.45	3.254(6)	145.2
C19–H19A···O16^{v}	0.96	2.31	3.194(12)	153.3
C30–H30A···O10^{v}	0.96	2.58	3.494(10)	159.7
C4–H4···O11^{vi}	0.93	2.49	3.214(9)	135.1
C24–H24···O20^{vii}	0.93	2.53	3.447(11)	168.1

[a] Symmetry transformations used to generate equivalent atoms: (i) 1 – *x*, 1 – *y*, 1 – *z*; (ii) 1 – *x*, – *y*, 1 – *z*; (iii) 1 – *x*, – *y*, – *z*; (iv) *x*, 1 + *y*, *z*; (v) *x*, –1 + *y*, *z*; (vi) 2 – *x*, 1 – *y*, –*z*; (vii) 2 – *x*, –*y*, 1 – *z*.

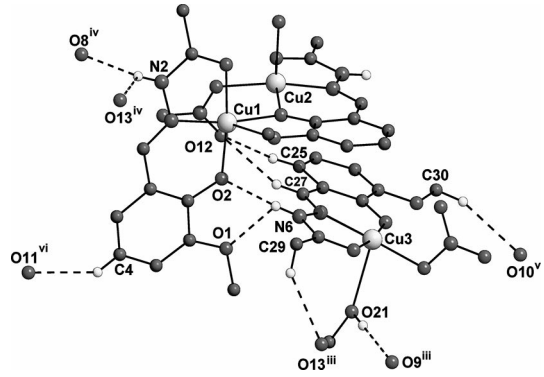

Figure 4. View of the asymmetric unit of **1** showing the intermolecular hydrogen-bonding interactions (dashed lines) between the dinuclear cation and the neutral mononuclear complex molecule. Hydrogen atoms not involved in hydrogen bonding, the free nitrate anion and water molecules, and the minor components of disorder are omitted for clarity. Symmetry codes: (iii) 1 – *x*, –*y*, –*z*; (iv) *x*, 1 + *y*, *z*; (v) *x*, –1 + *y*, *z*; (vi) 2 – *x*, 1 – *y*, –*z*.

A packing diagram showing the hydrogen-bonding interactions as dashed lines is presented in Figure 5 (a,b). In the asymmetric unit, the dinuclear cationic and the mononuclear neutral complexes are linked by intermolecular hydrogen bonds, where the N6–H6N···O1 and N6–H6N···O2 interactions (involving the protonated hydrazone nitrogen atom of the neutral complex molecule) constitute a pair of bifurcated donor bonds generating a ring of graph set $R^2_1(5)$,[15,16] and the C25–H25···O12 and C27–H27···O12 interactions (involving one oxygen atom of the nitrate group coordinated to atom Cu2) together form a pair of bifurcated acceptor bonds defining a ring of graph set $R^1_2(6)$.

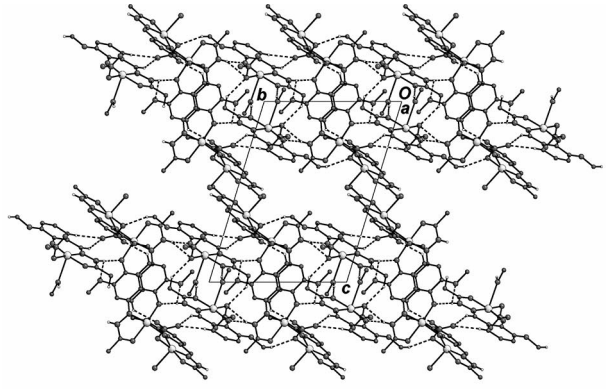

(a)

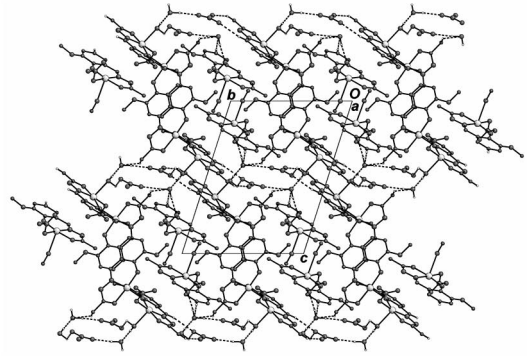

(b)

Figure 5. (a) Packing diagram of **1** showing the channels parallel to the *a*-axis formed by the three-dimensional hydrogen-bonded (dashed lines) framework of dinuclear cations and mononuclear complex molecules. Free nitrate anions and water solvent molecules hosted in the channels are omitted. Hydrogen atoms not involved in hydrogen bonds and the minor component of disorder are also omitted for clarity. (b) Packing diagram of **1** showing the nitrate anions and water solvent molecules hosted inside the channels. Hydrogen bonds involving nitrate anions and water molecules are shown as dashed lines. Hydrogen atoms not involved in hydrogen bonding and the minor components of disorder are omitted for clarity.

Adjacent asymmetric units are assembled into a three-dimensional network by C–H···O (C29–H29C···O13^{iii}, C30–H30A···O10^{v}, C4–H4···O11^{vi}) and O–H···O (O21–H21···O9^{iii}) hydrogen bonds, and by the N2–H2N···O8^{iv} and N2–H2N···O13^{iv} interactions constituting a pair of bifurcated donor bonds generating a ring of graph set $R^1_2(4)$ (Figure 4; symmetry codes given in the figure caption). In this arrangement, narrow channels running parallel to the *a*-axis are present (Figure 5, a), which accommodate the free nitrate anions and the disordered water molecules of crystallization (Figure 5, b). Atom O20 of the water molecule acts as both a hydrogen-bond donor to nitrate groups (O20–H20D···O18, O20–H20E···O15^{ii}; hereafter see Table 2 reporting the hydrogen-bonding interactions for symmetry codes) and as an acceptor to form O–H···O (O19–H19E···O20) and C–H···O interactions (C9–H9A···O20, C24–H24···O20^{vii}). The O16 and O17 oxygen atoms of the nitrate anion are engaged as acceptors in a bifurcated hydrogen bond involving the protonated hydrazone nitrogen atom of the dinuclear cationic complex (N4–H4N···O16^{v}, N4–H4N···O17^{v}) forming a ring of graph set $R^2_1(4)$, and are further involved in an O–H···O hydrogen interaction with the oxygen atom of the water molecule coordinated to Cu2 (O19–H19D···O17^{i}) and C–H···O interactions (C17–H17···O17^{v}, C19–H19A···O16^{v}).

[Mn$_2$(μ-L)$_2$(H$_2$O)(μ$_1$-N$_3$)$_2$(CH$_3$OH)] (2)

The noncentrosymmetric dinuclear unit of **2** is shown in Figure 6 and the selected bond lengths and angles are listed in Table 3. The asymmetric unit of **2** comprises of two non-equivalent seven-coordinated manganese(II) centers residing in nonidentical coordination spheres. The singly deprotonated tetradentate ONOO donor hydrazone ligand [**L**]$^-$ coordinates the two manganese centers via its ONOO donor sets (keto O, imine N, phenoxo O, and methoxy O), indicating that the ligand has not undergone enolization and coordinates the metal centers in keto form. Of the three oxygen atoms of [**L**]$^-$ only the phenoxo oxygen bridges the adjacent manganese(II) centers, while the keto and the methoxy oxygen coordinate Mn1 and Mn2 terminally. Unlike **1** in **2** the metal centers are "connected" via doubly phenoxo-bridges of the two units of [**L**]$^-$ (Figure 6) thereby generating a Mn_2O_2 core with a Mn···Mn distance of 3.490(1) Å, which is comparable to the earlier reported dinuclear phenolato-bridged manganese(II) complexes.[12] The Mn–O bond lengths in Mn_2O_2 core ranges from 2.172(3) Å to 2.222(3) Å. The average Mn–O–Mn bridge angle is slightly greater than that of the dinuclear phenolato-bridged octahedral manganese(II) complexes derived from phenol containing ligand with NNNNO donor sets: 104.54° vs. 103.7°.[12b] In **2** each manganese(II) center is surrounded by seven atoms: one (imine) nitrogen atom belonging to one [**L**]$^-$ ligand; one N_3^- ligand; five oxygen atoms [one (keto) oxygen atom, two (bridging phenoxo) oxygen atoms belonging to two [**L**]$^-$, one (methoxy) oxygen atom belonging to the other unit of [**L**]$^-$ coordinated to the adjacent manganese center and one from the solvent molecule (MeOH in case of Mn1 and H_2O for Mn2)].

The coordination of the methanol and the water molecule to the respective metal centers is responsible for the noncentrosymmetric character of **2**. The Mn–N bond lengths are in the range 2.310(4)–2.312(4) Å (given in Table 3) which is in good agreement with the Mn^{II}–N bond lengths where the nitrogen atom belongs to a phenolate-conjugated imine function.[12a] Both the manganese(II) centers are located in a regular bipyramid environment with a pentagonal base occupied by one nitrogen atom and four oxygen atoms of two units of [**L**]$^-$ (angles listed in Table 3). The latter is built from connecting oxygen atoms of the two ligands. The upper and lower states of the bipyramid come from terminally coordinated N_3^- ligands and coordinated solvent molecules. The noncentrosymmetric seven-coordinated manganese(II) dinuclear species are further connected to their adjacent units through H-bonding to gener-

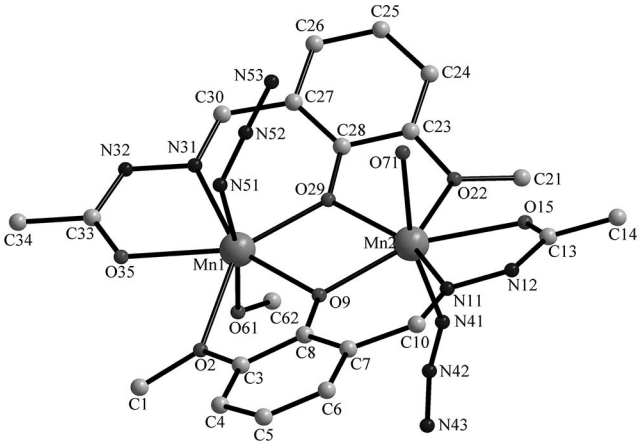

Figure 6. The noncentrosymmetric dinuclear asymmetric unit of **2**.

Table 3. Selected bond lengths [Å] and bond angles [°] for **2**.

Bond lengths		Bond lengths	
Mn1–O2	2.457 (4)	Mn2–N11	2.310 (4)
Mn1–O9	2.220 (4)	Mn2–O15	2.332 (4)
Mn1–O29	2.172 (3)	Mn2–O22	2.365 (4)
Mn1–N31	2.312 (4)	Mn2–O29	2.222 (3)
Mn1–O35	2.317 (3)	Mn2–N41	2.175 (5)
Mn1–N51	2.236 (4)	Mn2–O71	2.215 (4)
Mn1–O61	2.180 (4)	Mn1···Mn2	3.490 (1)
Mn2–O9	2.211 (4)	–	–
Bond angles	**[°]**	**Bond angles**	**[°]**
O2–Mn1–O9	67.6 (1)	O9–Mn2–N11	78.8 (2)
O2–Mn1–O29	141.2 (1)	O9–Mn2–O15	147.2 (1)
O9–Mn1–O29	75.9 (1)	N11–Mn2–O15	68.6 (2)
O2–Mn1–N31	140.3 (1)	O9–Mn2–O22	142.2 (1)
O9–Mn1–N31	151.9 (1)	N11–Mn2–O22	139.0 (2)
O29–Mn1–N31	77.6 (1)	O15–Mn2–O22	70.4 (1)
O2–Mn1–O35	70.9 (1)	O9–Mn2–O29	75.1 (1)
O9–Mn1–O35	136.8 (1)	N11–Mn2–O29	148.6 (1)
O29–Mn1–O35	147.2 (1)	O15–Mn2–O29	136.8 (1)
N31–Mn1–O35	69.7 (1)	O22–Mn2–O29	69.1 (1)
O2–Mn1–N51	94.5 (1)	O9–Mn2–N41	94.0 (2)
O9–Mn1–N51	86.2 (1)	N11–Mn2–N41	98.7 (2)
O29–Mn1–N51	95.6 (1)	O15–Mn2–N41	87.7 (2)
N31–Mn1–N51	87.3 (2)	O22–Mn2–N41	81.1 (2)
O35–Mn1–N51	85.8 (1)	O29–Mn2–N41	100.1 (2)
O2–Mn1–O61	83.4 (1)	O9–Mn2–O71	100.1 (2)
O9–Mn1–O61	100.7 (2)	N11–Mn2–O71	83.9 (2)
O29–Mn1–O61	91.2 (1)	O15–Mn2–O71	80.3 (2)
N31–Mn1–O61	89.0 (2)	O22–Mn2–O71	87.8 (2)
O35–Mn1–O61	85.6 (2)	O29–Mn2–O71	83.9 (1)
N51–Mn1–O61	171.3 (2)	N41–Mn2–O71	165.8 (2)

ate supramolecular architecture. The hydrogen-bond parameters are listed in Table 4. The conformation of the complex molecule is stabilized by intramolecular O–H···N (O71–H24···N53) hydrogen-bonding interactions (Figure 7).

In the crystal structure, complex molecules are linked into chains running parallel to the *a*-axis (Figure 8, a) through two intermolecular O–H···N hydrogen bonds involving terminal nitrogen atoms of the azide groups (N43, N53) and the oxygen atoms of the methanol (O61) and

Table 4. Hydrogen bond parameters of **2**.

D–H···A	*d*(D–H) [Å]	*d*(H···A) [Å]	*d*(D···A) [Å]	∠ (DHA)°
O61–H6–N53	0.83	1.95	2.752	163
O71–H8–N43	0.82	1.97	2.785	171
N32–H9–N51	0.85	2.05	2.873	161
O71–H24–N53	0.81	2.17	2.976	176

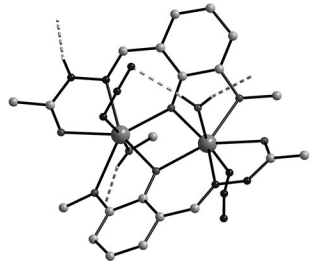

Figure 7. View of the asymmetric unit of **2** showing the intra- and intermolecular hydrogen-bonding interactions.

water (O71) molecules coordinated to Mn1 and Mn2, respectively. The chains are further connected into *zig-zag* layers parallel to the *ac* plane by N–H···N hydrogen-bonding interactions involving the N12 and N32 hydrazone ni-

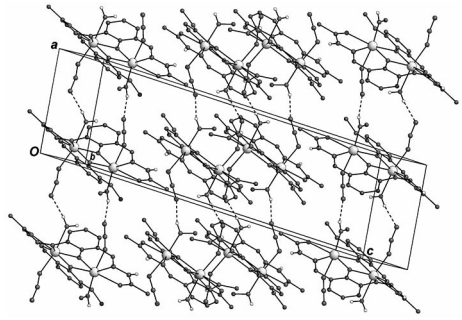

(a)

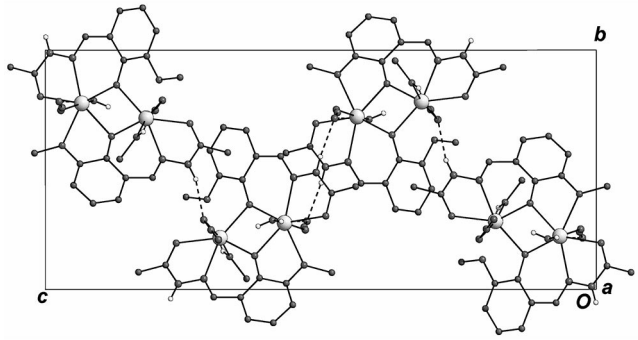

(b)

Figure 8. (a) Packing diagram of **2** showing the intermolecular N–H···N and O–H···N hydrogen bonds (dashed lines) linking complex molecules into chains running parallel to the *a*-axis. Hydrogen atoms not involved in hydrogen-bonding interactions are omitted for clarity. (b) Packing diagram of **2** viewed along the *a*-axis showing the *zig-zag* layer formation through N–H···N hydrogen-bonding interactions. Hydrogen atoms not involved in hydrogen-bonding interactions are omitted for clarity.

trogen atoms as H-donors and the N43 and N51 azide nitrogen atoms as acceptors, respectively (Figure 8, b). Unlike **1** no cavities or channels are present in the crystal lattice of **2**.

Spectroscopic Studies

IR Spectra: The IR spectra of **1** and **2** (Figure S1 and Figure S2) were analyzed in comparison with that of the free ligand [**LH**] (Figure S3) in the region 4000–400 cm^{-1}. In the IR spectrum of the hydrazone ligand, an imine stretching band was obtained at 1609 cm^{-1} but for the complexes the characteristic imine band was observed at a lower stretching frequency (1582 cm^{-1} for **1** and 1577 cm^{-1} for **2**) than that of the free ligand [**LH**]. The shift of these bands upon complexation towards lower wave numbers indicates the coordination of the imine nitrogen to the metal center.[17,18] The ligand also shows a strong carbonyl (C=O) stretching signal at 1681 cm^{-1} and a N–H stretching signal at 3187 cm^{-1}. Unlike other earlier reported metal hydrazone complexes, both of these bands were retained in the metal complexes but were shifted towards lower frequencies (1627, 3096 cm^{-1} for **1** and 1636, 3120 cm^{-1} for **2**), indicating that the hydrazone ligand has not undergone enolization and has coordinated the metal centers in keto form. The phenolic C–O stretching was observed in the spectra of the complexes at 1240 and 1277 cm^{-1} for **1** and at 1244 and 1285 cm^{-1} for **2**.[18] The coordination of the methoxy oxygen of [**L**]$^-$ in **1** and **2** is substantiated by the υ(C–O) bands appearing at 1010 cm^{-1} and 1015 cm^{-1}, respectively.[19] The IR spectra of **1** and **2** clearly support the coordination of the tetradentate ONOO donor hydrazone ligand [**L**]$^-$ to the respective metal centers [copper(II) and manganese(II)] via its carbonyl oxygen, imine nitrogen, phenolato oxygen, and methoxy oxygen atoms. Unlike **1**, in the spectrum of **2** a single nonbifurcated strong sharp band at 2069 cm^{-1} was observed which can be assigned to $\upsilon_{N=N}$ of the coordinated azide group and unlike **2**, the spectrum of **1** contains a very strong band at 1384 cm^{-1} [$\nu_{asym}(NO_3)$], and a medium band at 1240 cm^{-1} [$\nu_{sym}(NO_3)$] which supports the presence of a coordinated nitrate ion in the complex. In the spectra of **1** and **2** a broad band at 3422 cm^{-1} and 3400 cm^{-1} was observed which indicates the presence of water molecules in the crystal structures of the complexes. The ligand coordination to the respective metal centers is substantiated by υ_{M-N} bands appearing at 424 cm^{-1} for **1** and 407 cm^{-1} for **2**, where M = copper(II) for **1** and M = manganese(II) for **2**.[19]

Electronic Spectra: UV/Vis spectra of the hydrazone ligand [**LH**] and its complexes were recorded at 300 K using solid samples (diffuse-reflectance technique). The electronic spectra of the free ligand [**LH**] is associated with two intraligand charge transfer (CT) bands at 286 and 226 nm (Figure S4) but for **1** and **2** three different CT bands at 368, 307, 230 and 300, 235, 205 nm are observed (Figure S5 and Figure S6). In **1** and **2** the bands obtained at 307, 230 nm and 235, 205 nm are assigned to L→L charge-transfer transitions; as the spectrum of the free ligand lacks a CT band in the region 300–400 nm it can be concluded that in **1** and **2** the CT bands obtained at 368 and 300 nm are associated with the L→M charge-transfer transitions. In comparison to the spectrum of the free ligand for **1**, a much weaker and less well-defined broad asymmetric band is observed at 680 nm which is assigned to the d–d transitions for a copper(II) complex with square-pyramidal geometry (Figure S5).[20] For **2** no d–d transition bands were detected as such d–d transitions for a d^5 manganese(II) system are of very low intensity, and hence not detectable.

^{1}H NMR Spectra: ^{1}H NMR spectroscopy has been used to extract information regarding the formation of the ligand **LH** and its coordination mode with the metal ions in **1** and **2**. It is generally seen that ^{1}H NMR spectra of the coordination complexes containing paramagnetic metal ions are broadened to some extent but for **1** and **2** fairly sharp and well-resolved spectra were obtained which may have arisen due to sufficiently short electronic relaxation time.[21a,21b,21c] Unlike the spectrum of **LH** the chemical shifts of the hyperfine-shifted signals of **1** and **2** appeared within a short range +2 to +15 ppm. For both complexes the signals due to the protons closer to the respective metal centers experience stronger paramagnetic effects and consequently they are the most downfield shifted. The spectra of **1** and **2** are almost superimposable but differ significantly from that of the free ligand [**LH**]. For **1** and **2** (containing copper(II) and manganese(II) centers) slight broadening in the ^{1}H NMR spectra was observed but in order to compare the spectra of **1** and

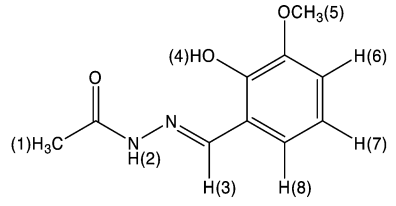

(a)

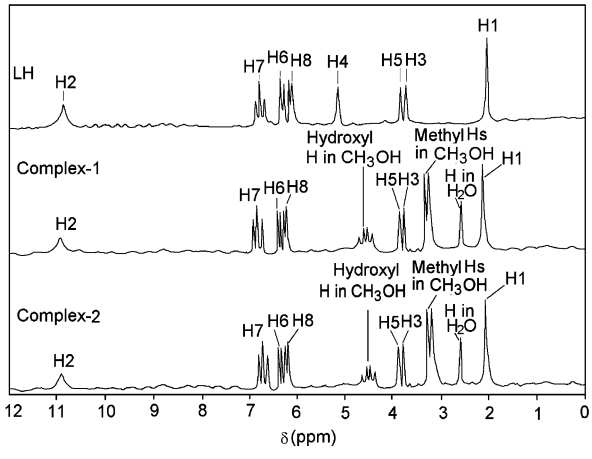

(b)

Figure 9. (a) NMR proton numbering scheme of **LH**. (b) Simulated ^{1}H NMR spectra of the hydrazone ligand [**LH**] and the complexes **1**, **2**.

Table 5. Simulated ^{1}H NMR spectroscopic data for the ligand **LH** and for complexes **1** and **2**.

Hydrazone ligand/complex	δ [ppm]
LH	2.0 (3 H, s, H1), 3.8 (1 H, s, H3), 3.86 (3 H, s, H5), 5.26 (1 H, s, H4), 6.35 (1 H, d, H8), 6.41 (1 H, d, H6), 6.80 (1 H, t, H7), 10.91 (1 H, s, H2)
1	2.02 (3 H, s, H1), 2.6 (2 H, s, H_2O), 3.4 (3 H, d, methyl Hs in CH_3OH), 3.82 (1 H, s, H3), 3.89 (3 H, s, H5), 4.5 (1 H, q, hydroxy H in CH_3OH), 6.39 (1 H, d, H8), 6.45 (1 H, d, H6), 6.86 (1 H, t, H7), 10.97 (1 H, s, H2)
2	2.01 (3 H, s, H1), 2.62 (2 H, s, H_2O), 3.41 (3 H, d, methyl Hs in CH_3OH), 3.8 (1 H, s, H3), 3.88 (3 H, s, H5), 4.51 (1 H, q, hydroxy H in CH_3OH), 6.38 (1 H, d, H8), 6.43 (1 H, d, H6), 6.85 (1 H, t, H7), 10.95 (1 H, s, H2)

2 with the free ligand [**LH**] we have simulated the spectra of the complexes. The NMR proton numbering scheme of **LH** along with the simulated ^{1}H NMR spectra of the ligand and the complexes are represented in Figure 9 (a,b) and the simulated ^{1}H NMR spectroscopic data are summarized in Table 5. In the NMR spectra of the free ligand **LH** the broad signal at 5–8 ppm was not observed indicating the absence of free $–NH_2$ functionality supporting the formation of the hydrazone ligand.[21d] In the spectrum of the free ligand a broad peak that appeared at δ = 10.91 ppm represented NH-proton resonance (H2) and this band was observed also in the spectra of complexes **1** and **2**. The broad band at δ = 10.91 ppm in **LH** was obtained at δ = 10.97 ppm in **1** and 10.95 ppm in **2** suggesting that the NH-proton (H2) did not participate in the keto–enol tautomerization and that the hydrazone ligand coordinated the metal ions in keto form.

Moreover, the signal for the enolic proton at 11–16 ppm in each of **LH**, **1**, and **2** was absent, supporting the fact that the hydrazone ligand did not undergo keto–enol tautomerization. The singlet due to the proton H(3) attached to the imino group showed a downfield shift (δ =0.02 ppm) compared to its position in the free ligand reflecting coordination of the ligand through the imine nitrogen. The signal due to the phenolic hydrogen (H4) of the free ligand (δ =5.26 ppm) was absent in the spectra of **1** and **2** indicating the coordination of the deprotonated phenolic oxygen to the metal center. The methoxy protons of the free hydrazone ligand are shifted 0.03–0.05 ppm downfield in the complexes which signifies that the methoxy oxygen participated in the coordination to the metal center. The aromatic hydrogens of **LH** showed significant shifts [0.04 ppm (H8), 0.04 ppm (H6), and 0.06 ppm (H9)] indicating the involvement of the phenolato oxygen in ligation with the metal center. In contrast to the spectrum of **LH** three additional peaks are obtained in the complexes. The doublet at 3.4–3.41 ppm and the quartet at 4.5–4.51 ppm are attributed to the methyl and hydroxy protons of a coordinated methanol molecule in **1** and **2**, respectively. Another singlet at 2.6–2.62 ppm is obtained for **1** and **2** which is attributed to the coordinated water molecule in the respective complexes.

Cryomagnetic Susceptibility Studies

The molar magnetic susceptibility χ_M as well as the product of molar magnetic susceptibility by temperature $\chi_M T$ have been plotted as a function of temperature T for **1** and are shown in Figure 10. χ_M continuously increases when the temperature decreases. The $\chi_M T$ value is about 1.17 $cm^3 K mol^{-1}$ at high temperature, in good agreement with the value of three uncoupled spins 1/2. $\chi_M T$ continuously decreases with a decrease of the temperature, a sign of the existence of an antiferromagnetic coupling inside the copper(II) dinuclear unit. At low temperature, $\chi_M T$ is about 0.44 $cm^3 K mol^{-1}$, a value expected for a single spin 1/2. As complex **1** is a mixture of a mononuclear and a dinuclear copper(II) complex, the $\chi_M T$ curve has been fitted with a modified Bleaney and Bowers law to take into account both moieties and using the phenomenological Hamiltonian $\mathbf{H} = -J\boldsymbol{S}_\mathbf{A}\boldsymbol{S}_\mathbf{B}$ for the dinuclear moiety. Two Landé factors have been assumed for the copper of the mononuclear (g_M) and dinuclear (g_D) moieties, respectively; see Equation (1).

$$\chi_M T = \frac{N\beta^2}{3k_B}\left[\frac{2g_D^2}{1+\exp\left(-J/k_B T\right)/3}+\frac{3}{4}g_M^2\right] \quad (1)$$

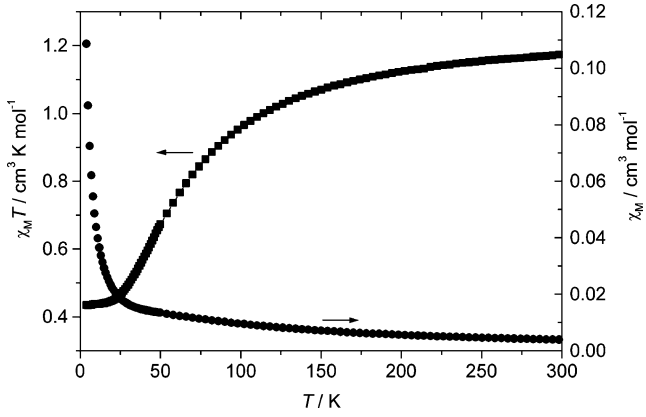

Figure 10. The plot of χ_M as well as $\chi_M T$ of **1** as a function of temperature.

The best fit was obtained with the following parameters: J = –84.2 cm^{-1}, g_D = 2.10 and g_M = 2.16. The values of g_D and g_M are in agreement with those derived by EPR spectra (mean g_D value of 2.13 and g_M value of 2.16). For the dinuclear unit, the antiferromagnetic interaction occurs through the oxygen atom of the singly phenoxo-bridged hydrazone ligand. Several articles have been devoted to the relation between the Cu–O–Cu angle and the J parameter from the experimental[22] and theoretical[23] point of view. The extrapolation of a linear relationship between J and the Cu–O–Cu angle, deduced from experimental data obtained

from Schiff base derivatives, suggests that ferromagnetic exchange should be found below the nonrealistic angle of 77°. More precisely, J is expected to decrease linearly with the Cu–O–Cu angle. Indeed, with a Cu–O–Cu angle of 110° the metal ions are coupled antiferromagnetically.

The molar susceptibility, χ_M of a powder sample of **2** was measured in the range 300–2 K in an applied magnetic field of 1 T. The experimental data are displayed in Figure 11 as the product $\chi_M T$ vs. temperature, T. The solid line in Figure 11 represents the simulation. At 300 K the $\chi_M T$ value is 9.12 $cm^3 K mol^{-1}$, which is only slightly higher than the theoretical "spin-only" value of 8.75 $cm^3 K mol^{-1}$ for two independent manganese(II) centers with $S = 5/2$ each. With decreasing temperature a decrease in the magnetic moment is observed, leading to a value of 1.31 $cm^3 K mol^{-1}$ at 2 K, indicating antiferromagnetic exchange interaction between the two high-spin manganese(II) ions; also this measurement is confirmed by EPR data. The best fit using the Heisenberg spin Hamiltonian in the form $\mathbf{H} = -J\boldsymbol{S}_A \cdot \boldsymbol{S}_B$ for an isotropic exchange coupling, with $\boldsymbol{S}_A = \boldsymbol{S}_B = 5/2$, is obtained with $g = 2.06$ and $J = -1.12$ cm^{-1}. These values are in agreement with those reported in the literature for complexes where two manganese(II) ions are bridged by two phenolates.[12,24–27]

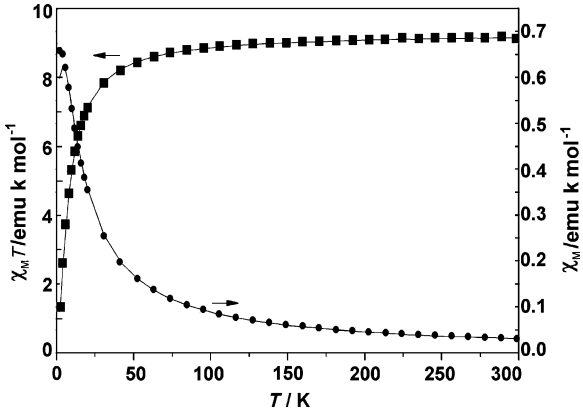

Figure 11. The plot of χ_M as well as $\chi_M T$ of **2** as a function of temperature.

DFT Calculations

In order to obtain some insight into the magnetic interaction, DFT calculations were carried out on both copper(II) and manganese(II) complexes (**1** and **2**). The calculated J values are –63.4 and –2.6 cm^{-1} for copper(II) and manganese(II) dinuclear species, respectively, and are in reasonable agreement with the experimental values (–84.2 and –1.12 cm^{-1}, respectively).

The magnetic orbitals for copper(II) in the dinuclear cationic unit are represented in Figure 12. Under the name of magnetic orbitals, we refer to the natural orbitals having an occupation number very close to 1. The two magnetic orbitals have a contribution on the two metal atoms. More precisely, this contribution is of the $d_{x^2-y^2}$ type, with the x- and y-axes being directed toward the four short metal–ligand bonds. These orbitals are also delocalized on the surrounding ligands. The interaction between the metal and the ligand is antibonding in nature, as expected from simple molecular orbital theory arguments. The fact that the two orbitals have a contribution on both metal centers means that there is a nonzero overlap between the so-called natural magnetic orbitals.[28] Following the so-called Kahn's model, such an overlap is expected to give rise to an antiferromagnetic interaction, as observed experimentally.

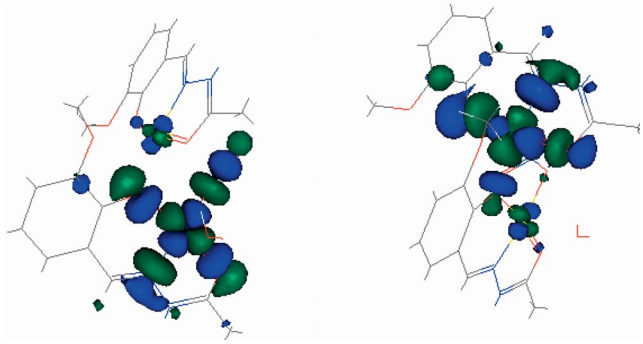

Figure 12. Magnetic orbitals for the high spin state of the dinuclear copper compound.

Concerning the manganese(II) dinuclear compound, five unpaired electrons are bared by each metal atom, so that the global interaction may be seen as the sum of 25 interactions. Some of these will be ferromagnetic in nature, some will be antiferromagnetic, so that in the end the small interaction observed may be explained by the compensation between the ferromagnetic and antiferromagnetic terms.

EPR Spectra

The X-band EPR spectrum of the polycrystalline solid complex **1** at 5 K is characterized by two g values ($g_\parallel$ = 2.278 and $g_\perp$ = 2.101) in the order $g_\parallel > g_\perp > g_e$ (Figure 13, a). This situation is indicative of a $S = 1/2$ system with an axial symmetry and a $d_{x^2-y^2}$ ground state.[20b,29,30] Other weak absorptions are observable at lower and higher values of the magnetic field.

The spectra recorded at liquid nitrogen temperature (ca. 120 K) or at room temperature become more complicated: other resonances appear and four g values (indicated with **I**, **II**, **III**, and **IV** in Figure 13, b) can be measured. They can be interpreted as the sum of the spectra belonging to weakly interacting copper(II) ions (see cryomagnetic studies). The experimental spectrum at 120 K can be satisfactorily simulated by adding three separated signals belonging to each of the three different copper(II) ions: the first with g_x = 2.305, g_y = 2.090, g_z = 2.033, the second with g_x = 2.260, g_y = 2.090, g_z = 2.025, and the third with $g_\parallel$ = 2.280, $g_\perp$ = 2.100. The simulation suggests that there are two copper(II) centers characterized by a rhombic symmetry and three g values ($g_x > g_y > g_z \approx g_e$), and another with an axial symmetry and $g_\parallel > g_\perp > g_e$.[20b,29,30]

Therefore, from the comparison of the results obtained at 5 and 120 K, the axial temperature-independent spectrum can be attributed to the mononuclear Cu3 center with

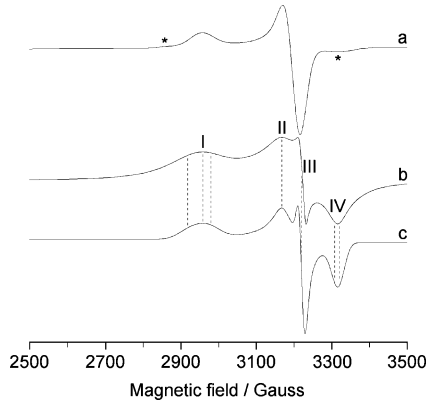

Figure 13. X-band EPR spectra of the polycrystalline solid complex **1**: (a) and (b) experimental spectra recorded at 5 and 120 K; (c) simulated spectrum. The simulated spectrum was obtained by adding three different spectra with the following g values: g_x = 2.305, g_y = 2.090 and g_z = 2.033; g_x = 2.260, g_y = 2.090 and g_z = 2.025; $g_\parallel$ = 2.280 and $g_\perp$ = 2.100. With an asterisk are indicated the resonances belonging to the Cu1 and Cu2 centers at 5 K, with **I**, **II**, **III**, and **IV** the four measurable g values at 120 K and with the dotted lines the positions of the eight transitions due to the three metal ions.

a regular square-pyramidal environment, whereas the two rhombic spectra can be attributed to the Cu1 and Cu2 ions which form the dinuclear arrangement and show a distorted square-pyramidal geometry. Owing to the antiferromagnetic interaction between Cu1 and Cu2, at 5 K the S = 1 spin state scarcely contributes to the spectral signal and only the weak resonances centered around 2850 and 3320 Gauss (indicated by an asterisk in Figure 13, a) are observable; at higher temperatures both the S = 0 and 1 states are populated and the EPR spectrum appears as the sum of the signals belonging to the different Cu1, Cu2, and Cu3 metal centers.

X-band anisotropic EPR spectra of complex **1** were also recorded after dissolution in the mixture $CHCl_3$/toluene (60:40, v/v; under similar conditions to the NMR studies), or in DMF or CH_3CN. Whereas in $CHCl_3$/toluene **1** is poorly soluble and the spectrum is similar to that of polycrystalline powder, suggesting that the structure is retained, in DMF or CH_3CN the spectra are axial and characteristic of species with S = 1/2 (Figure 14). The comparison of the spectral intensity of such mononuclear complexes with that of aquaion $[Cu(H_2O)_6]^{2+}$ in a solution containing an identical concentration of the metal ion allows for determining that the dinuclear structure is transformed almost quantitatively into the mononuclear complexes and that its amount in DMF or CH_3CN solution is lower than 5%.

The measured values in DMF (Figure 14, a) are $g_\parallel$ = 2.286 and $A_\parallel$ = 175.1×10^{-4} cm^{-1}, compatible with a CuONOO coordination:[31] each copper(II) ion is coordinated by one tridentate ligand ($O^-_{phenolic}$, N_{imine}, O_{keto}) and one nitrate ion. The distortion degree of such a four-coordinate copper(II) complex from a square-planar geometry can be measured by the $g_\parallel/A_\parallel$ ratio, which increases with increasing the value of the tetrahedral distortion:[32] the observed ratio for **1** in DMF (131) suggests a significant distortion

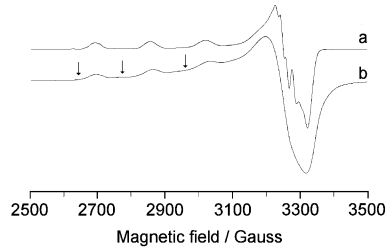

Figure 14. X-band EPR spectra recorded at 120 K with the solid complex **1** dissolved in: a) DMF and b) CH_3CN. The arrows indicate the resonances of a second mononuclear copper(II) species.

with respect to a structure with a high level of planarity, such as the bis-chelated species formed by 2-(aminomethyl)-pyridine (112).[33] In CH_3CN (Figure 14, b), besides the resonances of a species similar to that detected in DMF ($g_\parallel$ = 2.280 and $A_\parallel$ = 181.8×10^{-4} cm^{-1}), there are those of another mononuclear complex with higher $g_\parallel$ and lower $A_\parallel$ values (indicated by the arrows in Figure 14, b): $g_\parallel$ = 2.354 and $A_\parallel$ = 174.1×10^{-4} cm^{-1}. These values are border-line for a CuN_3O coordination,[31] and can be better explained by postulating a tetra-coordinated structure CuN_2O_2 in which one solvent molecule has replaced one NO_3^- ion.

As known, the magnetic spin levels of manganese(II) can be described by the spin Hamiltonian; see Equation (2).[34]

$$\hat{H} = g\beta H\hat{S} + 1/2D[\hat{S}_z^2 - 1/3S(S+1)] - E[\hat{S}_x^2 - \hat{S}_y^2] - A\hat{S}\cdot\hat{I} - g_N\beta_N H\hat{I} \quad (2)$$

The X-band EPR spectra recorded at 120 K with the polycrystalline solid complex **2** and when this is dissolved in the mixture $CHCl_3$/toluene (60:40, v/v) or in MeOH are shown in Figure 15.

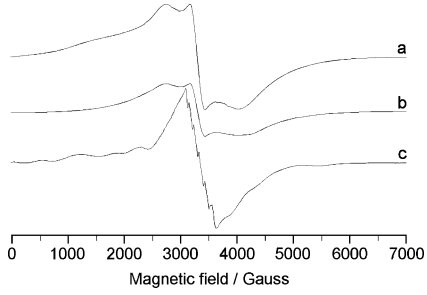

Figure 15. X-band EPR spectra recorded at 120 K of complex **2**: (a) polycrystalline powder; (b) solid dissolved in $CHCl_3$/toluene (60:40, v/v) and (c) solid dissolved in MeOH.

The high linewidth precludes a precise analysis of the spectrum at 120 K (Figure 15, a), but the spectral pattern closely resembles that displayed by other weakly exchange-coupled manganese(II) dinuclear species formed by a Schiff base ligand like salmp = 2-[bis(salicyldeneamino)methyl]-phenolate(3–)[35,36] and 2-OH(5-NO_2sal)pn = 5-nitro-1,3-bis(salicyldeneamino)-2-propanol(3–),[37] where two phenolate groups bridge two manganese(II) ions.

A method based on the examination of the variation of the experimental spectra as a function of temperature, in order to assign the transitions between the relevant spin states and the spin parameters, has been recently devel-

oped.[38] The X-band EPR spectra recorded between 0 and 8000 Gauss in the temperature range 5–25 K are shown in Figure 16. All spectra exhibit features extending from 0 to 6000 Gauss; as the temperature is increased, both the whole spectrum and the transitions around $g = 2$ gain intensity. This behavior is strongly indicative of dinuclear manganese(II) species.[12,24,39] The spectra significantly change from 5 to 15 K and less above 15 K. Because of the low value of the exchange coupling constant ($J = -1.12\ cm^{-1}$) and the small gap between S spin levels at zero field, the $S = 1$–3 states, even at liquid helium temperature, are significantly populated and the spectrum recorded at 5 K originates from the participation of, at least, three states. With the temperature, increases also the contribution of $S = 4$ and $S = 5$ spin states; in particular, the appearance of the intense transitions detected in the $g = 2$ region from 5 to 25 K should confirm that the experimental signal is the superimposition of the spectra belonging to the $S = 1$–5 states. Similar behavior was observed for other weakly antiferromagnetically coupled dinuclear manganese complexes with a low J value.[12b] The complexity of the spectral pattern precludes a precise determination of the D parameter and the resolution of the $S = 1$–5 temperature-independent spectra.

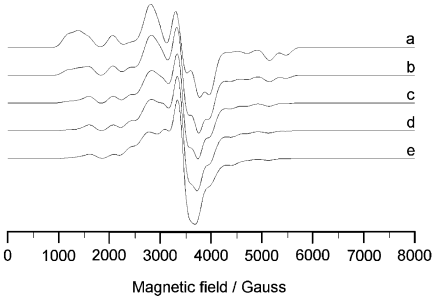

Figure 16. X-band EPR spectra recorded as a function of temperature for complex **2**: a) 5 K; b) 10 K; c) 15 K; d) 20 K and e) 25 K.

The EPR spectrum of **2** dissolved in $CHCl_3$/toluene (60:40, v/v) closely resembles that recorded in the solid state, confirming the NMR results which suggest that in a noncoordinating solvent the dinuclear arrangement is preserved (Figure 15, b). In MeOH, instead, the spectrum is typical of mononuclear manganese(II) species with weak zero-field splitting (Figure 15, c).[40] The spectrum is characterized by a strong signal centered at 3280 G with a value of $g \approx 2.05$; sixfold well-resolved hyperfine splitting of central transitions ($M_s = -1/2 \rightarrow 1/2$) is observable, owing to the hyperfine interaction between the electron and nuclear spin ($I = 5/2$) which splits all of the energy levels associated to each M_s value into six sublevels.[41] In order to understand if these features are due to a mono- or a dinuclear species a further spectrum has been recorded at 5 K: the similarity of the spectral pattern with that observed at 120 K induces us to think that the dinuclear structure is almost completely destroyed in MeOH, similarly to what happens for **1** in DMF and CH_3CN. The hyperfine coupling constant A of 93.2 Gauss is consistent with a six-coordinate manganese(II) species with oxygen or nitrogen donors.[41] This spectral pattern suggests that the dinuclear structure dissociates in a coordinating solvent giving rise to the mononuclear unit.

Conclusions

In this paper we have explored the coordination behavior of a potentially tetradentate ONOO donor hydrazone ligand with two different metal ions. It is interesting to conclude that the ligand [**LH**] has shown a considerable amount of selectivity in its coordination behavior with two different metal ions [copper(II), manganese(II)]. It is observed, for copper(II) ions preferring square-pyramidal geometry, that the hydrazone ligand has coordinated the metal centers in tridentate as well as in tetradentate fashion to generate an asymmetric unit comprising of an unusual singly phenoxo-bridged dinuclear cationic unit associated with a neutral unit. For seven-coordinated manganese(II) ions residing in a pentagonal-bipyramidal environment the ligand coordinates via its tetradentate mode and generates a doubly phenoxo-bridged manganese(II) dinuclear species. The extensive ligand-based hydrogen-bonding interactions in the respective complexes have resulted in the two new intriguing 3D supramolecular architectures. The cryomagnetic investigations on **1** and **2** suggest that both complexes are antiferromagnetically coupled and the J values ($-63.4\ cm^{-1}$ and $-2.6\ cm^{-1}$) obtained from DFT calculations are in reasonable agreement with the experimental results. EPR spectra of **1** and **2** recorded after dissolution in a mixture of $CHCl_3$/toluene, or in DMF or CH_3CN help us to conclude that the dinuclear structures of the respective complex are retained in a noncoordinating solvent ($CHCl_3$/toluene) whereas in coordinating solvents (DMF, CH_3CN, or MeOH) both the complexes degrade to produce mononuclear species.

Experimental Section

Instrumentation: The Fourier Transform Infrared spectra of the hydrazone ligand [**LH**] and the complexes were recorded with a Perkin–Elmer Spectrum RX I FT-IR system in the range 4000–400 cm^{-1} with solid KBr disc. Ligand field spectra were obtained from 800 to 200 nm at 300 K with a Perkin–Elmer λ-40 UV/Vis-spectrometer by using the diffuse-reflectance technique, with Nujol mulls. C,H,N microanalyses were carried out with a Perkin–Elmer 2400 II elemental analyzer. ^1H NMR spectra of the ligand and the complexes were recorded with a Bruker 300 MHz FT-NMR spectrometer using trimethylsilane as an internal standard in $CDCl_3$. Mass spectra of the ligand [**LH**] were recorded with a Qtof Micro YA mass spectrophotometer. The variable-temperature magnetic susceptibility measurement for **1** was carried out with a Quantum Design MPMS-5S SQUID magnetometer under an applied magnetic field of 5000 Oe. Diamagnetic corrections were estimated from Pascal tables and magnetic data were corrected for diamagnetic contributions of the sample holder. The temperature dependence of the molar magnetic susceptibility, χ_M, was measured on a polycrystalline sample in the temperature range 4–300 K. The

experimental points are drawn in black squares and the calculated curves are marked by a solid line (see Figures 10, 11). All the data analyses have been placed on the $\chi_M T$ plots. Magnetic susceptibility data for polycrystalline sample **2** were collected in the temperature range 2–290 K in an applied magnetic field of 1 T with a SQUID magnetometer. Experimental susceptibility data were corrected for the underlying diamagnetism using Pascal's constants and for the temperature-independent paramagnetism contributions. EPR spectra of **1** and **2** were recorded for the polycrystalline powders or for the solids dissolved in a mixture of $CHCl_3$/toluene (60:40, v/v), or in DMF, CH_3CN, or MeOH with an X-band (9.35 GHz) Bruker EMX spectrometer at room temperature, 120 K, or in the range 5–25 K. The addition of toluene to $CHCl_3$ was necessary to ensure a good glass formation. For low-temperature studies (5–25 K), an Oxford Instrument continuous-flow liquid helium cryostat and a temperature-control system were used. The spectra were simulated with the computer program Bruker WinEPR SimFonia.[42]

Chemicals: All chemicals and solvents used for the syntheses were of analytical grade. Acethydrazide, vanillin, copper nitrate trihydrate, manganese nitrate tetrahydrate, and sodium azide were purchased from Aldrich Chemical Co. and were used without further purification.

Synthesis of the Hydrazone Ligand [LH]: The ligand **LH** was prepared by the condensation of acethydrazide (0.74 g, 10 mmol) with vanillin (1.525 g, 10 mmol) in the presence of glacial acetic acid (0.6 mL, 10 mmol) in methanol medium (200 mL). On refluxing the methanolic solution for 5 h a pale yellow coloration was observed. The color indicated the formation of the hydrazone ligand **LH**. The solvent was removed under reduced pressure and the residue was purified by recrystallization. Pale yellow crystals, yield 0.181 g (87%). $C_{10}H_{12}N_2O_3$ (208.21): calcd. C 57.63, H 5.76, N 13.45; found C 57.68, H 5.78, N 13.49. Mass spectrum (EI): *m/e* 231 $[C_{10}H_{12}N_2NaO_3]^+$. IR (KBr): $\tilde{\nu}$ = ν(C=N) 1609 cm^{-1}, ν(C=O) 1681 cm^{-1}, ν(N–H) 3187 cm^{-1}. ^1H NMR: δ = 2.0 (s, 3 H, H1), 3.8 (s, H3, 1 H), 3.86 (s, H5, 3 H), 5.26 (s, H4, 1 H), 6.35 (d, H8, 1 H), 6.41 (d, 1 H, H6), 6.80 (t, H7, 1 H), 10.91 (s, 1 H, H2) ppm.

Syntheses of the Complexes

$\{[(L)Cu_2(\mu\text{-}L)(NO_3)(CH_3OH)_{0.3}(H_2O)_{0.7}]\cdot NO_3\}[Cu(L)(NO_3)(CH_3OH)]$ (1): The pale yellow, solid hydrazone ligand (0.416 g, 2 mmol) was weighted accurately and was stirred in methanol (10 mL) to give a pale yellow solution. It was then added slowly to a stirring solution of methanolic copper nitrate trihydrate (15 mL) (0.723 g, 3 mmol) to give a light green solution. The light green solution was then refluxed at 60 °C for 1 h which produced a darker shade. Acetonitrile (10 mL) was added to the dark green solution and further stirred for 2 h at 35 °C. The resulting solution was filtered and the filtrate was kept at 20 °C yielding dark green plate-shaped crystals suitable for X-ray diffraction after three weeks. Crystals were isolated by filtration and were air-dried; yield 0.622 g (86%). $C_{31.3}H_{41}Cu_3N_9O_{20.7}$ (1065.15): calcd. C 35.26, H 3.85, N 11.83; found C 35.28, H 3.89, N 11.87. IR (KBr): $\tilde{\nu}$ = ν(C=N) 1582 cm^{-1}, $\nu(C{=}O)_{carbonyl}$ 1627 cm^{-1}, $\nu(C{-}O)_{phenolic}$ 1240 and 1277 cm^{-1}, $\nu(C{-}O)_{methoxy}$ 1010 cm^{-1}, ν(N–H) 3096 cm^{-1}, $\nu_{asym}(NO_3)$ 1384 cm^{-1}, $\nu_{sym}(NO_3)$ 1240 cm^{-1}, ν(O–H) 3422 cm^{-1}, ν(Cu–N) 424 cm^{-1}.

$[Mn_2(\mu\text{-}L)_2(H_2O)(\mu_1\text{-}N_3)_2(CH_3OH)]$ (2): The pale yellow solution of the hydrazone was obtained by stirring solid **LH** (0.208 g, 1 mmol) in methanol (15 mL). It was then slowly added to a methanolic solution of manganese nitrate tetrahydrate (15 mL) (0.251 g, 1 mmol) and was stirred for 20 min which resulted in an orange coloration. After dropwise addition of an aqueous solution of sodium azide (5 mL) (0.065 g, 1 mmol) the orange solution took a darker shade. It was then further stirred for 2 h at 35 °C in anaerobic conditions to produce a dark red solution. The resulting solution was filtered and the filtrate was kept at 18 °C yielding yellow plate-shaped crystals suitable for X-ray diffraction after two weeks. Crystals were isolated by filtration and were air-dried; yield 0.206 g (82%). $C_{21}H_{28}Mn_2N_{10}O_8$ (658.4): calcd. C 38.27, H 4.25, N 21.26; found C 38.29, H 4.29, N 21.29. IR (KBr): $\tilde{\nu}$ = ν(C=N) 1577 cm^{-1}, $\nu(C{=}O)_{carbonyl}$ 1636 cm^{-1}, $\nu(C{-}O)_{phenolic}$ 1244 and 1285 cm^{-1}, $\nu(C{-}O)_{methoxy}$ 1015 cm^{-1}, ν(N–H) 3120 cm^{-1}, ν(N=N) 2069 cm^{-1}, ν(O–H) 3400 cm^{-1}, ν(Mn–N) 407 cm^{-1}.

Crystal Structure Determination: The intensity data of **1** were collected with a Bruker SMART 1000 CCD, using the ω-scan technique. Data collection and data reduction were performed with the SMART and SAINT programs.[43] Empirical absorption corrections were carried out using the SADABS program.[44] The structures were solved by direct methods by using the SHELXS-97 program.[45] All non-hydrogen atoms were refined anisotropically by full-matrix least-squares based on F^2 using the SHELXL-97 program.[45] All non-hydrogen atoms were refined with anisotropic displacement parameters. The H atoms were generated geometrically and were included in the refinement in the riding model approximation. The apical position of the square-pyramidal coordination around Cu2 was found to be statistically occupied by the oxygen atom belonging to a water molecule and to a methanol molecule with occupancies of 0.7 and 0.3, respectively. A second water molecule, the presence of which was not compatible with the methanol molecule, was therefore refined with an occupancy of 0.7. During the refinement, the displacement parameters of the atoms of the methanol and water molecules were restrained to be approximately isotropic. Single-crystal X-ray studies of **2** were carried out using a Nonius KappaCCD and related analysis software.[46] No absorption correction was applied to the data sets of all the samples. The structure was solved by direct methods using the SIR97 program[47] combined to Fourier difference syntheses and refined against F using reflections with $[I/\sigma(I) > 3]$ with the CRYSTALS program.[48] All atomic displacement parameters for non-hydrogen atoms were refined with anisotropic terms. The hydrogen atoms were theoretically located on the basis of the conformation of the supporting atom and then refined to find their real position keeping some constraints belonging to the supported atoms. Selected crystallographic data, experimental conditions, and some important features of the structural refinements of the complexes are summarized in Table 6.

CCDC-664106 (for **1**), and -664107 (for **2**) contain the supplementary crystallographic data for this paper. These data can be obtained free of charge from The Cambridge Crystallographic Data Centre via www.ccdc.cam.ac.uk/data_request/cif.

DFT Methodology: The calculated coupling constant J is deduced from two separate DFT computations carried out for the highest spin state and for the broken symmetry state. The hybrid B3LYP[49] functional has been used as implemented in Gaussian98.[50] The basis used in all calculations is the triple-ζ basis-set proposed by Ahlrichs et al.[51] for transition metals and the double-ζ basis set proposed by the same authors for the other atoms.[52] The obtained J values are deduced from the energy difference $E_{HS} - E_{BS} = -J(2S_1S_2 + S_2)$ where E_{HS} and E_{BS} are the energies of high spin and broken symmetry states, respectively, S_1 and S_2 being the spin of the two metals involved ($S_1 = S_2 = 1/2$ for the copper(II) dinuclear species, $S_1 = S_2 = 5/2$ for the manganese(II) dinuclear species). We assume that the energy of the broken symmetry state is a good approximation of low-spin state energy, following Ruiz et al.[53]

Table 6. Crystal data and structure refinement for **1** and **2**.

	1	**2**
Empirical formula	$C_{31.3}H_{41}Cu_3N_9O_{20.7}$	$C_{21}H_{28}Mn_2N_{10}O_8$
Formula weight	1065.15	658.4
Temperature [K]	302	150
Wavelength [Å]	0.71073	0.71073
Crystal system	triclinic	monoclinic
Space group	$P\bar{1}$ (no. 2)	$P2_1/n$
a [Å]	11.495(4)	8.3409 (2)
b [Å]	12.662(5)	11.8465 (2)
c [Å]	16.562(6)	28.0454 (6)
α [°]	69.223(4)	90
β [°]	75.613(5)	97.638 (1)
γ [°]	70.495(4)	90
Volume [Å^3]	2101.2(13)	2746.6 (1)
D_c [g cm^{-3}]	1.684	1.592
Abs. coefficient [mm^{-1}]	1.597	0.984
F(000)	1089	1352
Crystal size [mm]	0.06 × 0.07 × 0.26	0.10 × 0.12 × 0.14
θ range for data collection	1.8, 25.8°	1.5, 27.9°
Reflections collected	20411	35371
Independent reflections	7987 [R(int) = 0.069]	3074 [R(int) = 0.130]
Data/restraints/parameters	7987, 83, 584	307, 0, 370
Goodness-of-fit on F^2	0.906	1.13
$R1$, $wR2$[a] [$I > 2\sigma(I)$]	0.051, 0.106	0.050, 0.058
$R1$, $wR2$[a] (all data)	0.146, 0.130	0.107, 0.116

[a] $R_1 = \Sigma||F_o| - |F_c||/\Sigma|F_o|$; $wR_2 = [\Sigma w(F_o^2 - F_c^2)^2/\Sigma w(F_o^2)^2]^{1/2}$.

Supporting Information (see also the footnote on the first page of this article): IR spectra of the new hydrazone ligand [**LH**] and its complexes **1** and **2** and UV/Vis spectra (diffuse-reflectance technique) of **LH**, **1**, and **2**.

Acknowledgments

A. Ray is thankful to the Council of Scientific and Industrial Research, New Delhi, Government of India, for providing her with the financial support to carry out the work. The authors also acknowledge the financial help obtained from All India Council for Technical Education, New Delhi, Government of India.

[1] a) V. Chandrasekhar, R. Azhakar, G. T. S. Andavan, V. Krishnan, S. Zacchini, J. F. Bickley, A. Steiner, R. J. Butcher, P. Kögerler, *Inorg. Chem.* **2003**, *42*, 5989–5998; b) N. M. H. Salem, L. El-Sayed, M. F. Iskander, *Polyhedron* **2008**, *27*, 3215–3226; c) S. Naskar, D. Mishra, R. J. Butcher, S. K. Chattopadhyay, *Polyhedron* **2007**, *26*, 3703–3714.

[2] a) R. Pedrido, M. J. Romero, M. R. Bermejo, A. M. González-Noya, M. Maneiro, M. Jesús Rodríguez, G. Zaragoza, *Dalton Trans.* **2006**, 5304–5314, and references cited therein; b) N. R. Sangeetha, S. Pal, *Polyhedron* **2000**, *19*, 1593–1600, and references cited therein; c) S. Banerjee, A. Ray, S. Sen, S. Mitra, D. L. Hughes, R. J. Butcher, S. R. Batten, *Inorg. Chim. Acta* **2008**, *361*, 2692–2700, and references cited therein; d) S. Banerjee, S. Sen, S. Basak, S. Mitra, D. L. Hughes, C. Desplanches, *Inorg. Chim. Acta* **2008**, *361*, 2707–2714; e) B. Samanta, J. Chakraborty, S. Shit, S. R. Batten, P. Jensen, J. D. Masuda, S. Mitra, *Inorg. Chim. Acta* **2007**, *360*, 2471–2484; f) S. Sen, C. R. Choudhury, P. Talukder, S. Mitra, M. Westerhausen, A. N. Kneifel, C. Desplanches, N. Daro, J.-P. Sutter, *Polyhedron* **2006**, *25*, 1271–1278; g) S. Sen, S. Mitra, D. L. Hughes, G. Rosair, C. Desplanches, *Polyhedron* **2007**, *26*, 1740–1744.

[3] S. Naskar, M. Corbella, A. J. Blake, S. K. Chattopadhyay, *Dalton Trans.* **2007**, 1150–1159.

[4] a) D. Braga, F. Grepioni, G. R. Desiraju, *Chem. Rev.* **1998**, *98*, 1375–1405; b) D. Braga, F. Grepioni, *Coord. Chem. Rev.* **1999**, *183*, 19–41; c) D. Braga, F. Grepioni, *Acc. Chem. Res.* **2000**, *33*, 601–608; d) N. J. Burke, A. D. Burrows, A. S. Donovan, R. W. Harrington, M. F. Mahon, C. E. Price, *Dalton Trans.* **2003**, 3840–3849; e) D. M. P. Mingos, M. Alajarin, A. E. Aliev, A. D. Burrows, K. D. M. Harris, A. Pastor, J. W. Steed, D. R. Turner, *Supramolecular Assembly via Hydrogen Bonds*, vol. 1, Springer, Berlin, **2004**.

[5] a) J.-M. Lehn, *Supramolecular Chemistry, Concepts and Perspectives*, VCH, New York, **1995**; b) J. W. Steed, J. L. Atwood, *Supramolecular Chemistry*, John Wiley & Sons, New York, **2000**; c) A. M. Beatty, *Coord. Chem. Rev.* **2003**, *246*, 131–143; d) H. W. Roesky, M. Andruh, *Coord. Chem. Rev.* **2003**, *236*, 91–119; e) B. J. Holliday, C. A. Mirkim, *Angew. Chem. Int. Ed.* **2001**, *40*, 2022–2043.

[6] a) M. Eddaoudi, D. B. Moler, H. Li, B. Chen, T. M. Reineke, M. O'Keeffe, O. M. Yaghi, *Acc. Chem. Res.* **2001**, *34*, 319–330; b) M. Eddaoudi, J. Kim, N. Rosi, D. Vodak, J. Wachter, M. O'Keeffe, O. M. Yaghi, *Science* **2002**, *295*, 469–472.

[7] a) S. Kitagawa, R. Kitaura, S. Noro, *Angew. Chem. Int. Ed.* **2004**, *43*, 2334–2375; b) R. Kitaura, S. Kitagawa, Y. Kubota, T. C. Kobayashi, K. Kindo, Y. Mita, A. Matsuo, M. Kobayashi, H. C. Chang, T. C. Ozawa, M. Suzuki, M. Sakata, M. Takata, *Science* **2002**, *298*, 2358–2361.

[8] a) S. S. Y. Chui, S. M. F. Lo, J. P. H. Charmant, A. G. Orpen, I. D. Williams, *Science* **1999**, *283*, 1148–1150; b) L. Pan, K. M. Adams, H. E. Hernandez, X. Wang, C. Zheng, Y. Hattori, K. Kaneko, *J. Am. Chem. Soc.* **2003**, *125*, 3062–3067.

[9] a) J. Veciana, J. Cirujeda, C. Rovira, E. Molins, J. J. Novoa, *J. Phys. I Fr.* **1996**, *6*, 1967–1986; b) D. B. Leznoff, B.-Y. Xue, C. L. Stevens, A. Storr, R. C. Thompson, B. O. Patrick, *Polyhedron* **2001**, *20*, 1247–1254.

[10] A. Ray, S. Banerjee, R. J. Butcher, C. Desplanches, S. Mitra, *Polyhedron* **2008**, *27*, 2409–2415.

[11] C. R. Choudhury, S. K. Dey, R. Karmakar, C.-D. Wu, C.-Z. Lu, M. S. El Fallah, S. Mitra, *New J. Chem.* **2003**, *27*, 1360–1366.

[12] a) C. Hureau, E. Anxolabéhère-Mallart, M. Nierlich, F. Gonnet, E. Rivière, G. Blondin, *Eur. J. Inorg. Chem.* **2002**, 2710–2719, and references cited therein; b) L. Sabater, C. Hureau, G. Blain, R. Guillot, P. Thuéry, E. Rivière, A. Aukauloo, *Eur. J. Inorg. Chem.* **2006**, 4324–4337, and references cited therein; c) C. Hureau, L. Sabater, E. Anxolabéhère-Mallart, M. Nierlich, M.-F. Charlot, F. Gonnet, E. Rivière, G. Blondin, *Chem. Eur. J.* **2004**, *10*, 1998–2010.

[13] O. Pouralimardan, A.-C. Chamayou, C. Janiak, H. Hosseini-Monfared, *Inorg. Chim. Acta* **2007**, *360*, 1599–1608.

[14] J. Chakraborty, S. Thakurta, G. Pilet, D. Luneau, S. Mitra, *Polyhedron* **2009**, *28*, 819–825.

[15] J. Bernstein, R. E. Davis, L. Shimoni, N.-L. Chang, *Angew. Chem. Int. Ed. Engl.* **1995**, *34*, 1555–1573.

[16] M. C. Etter, *Acc. Chem. Res.* **1990**, *23*, 120–126.

[17] L. J. Farrugia, *J. Appl. Crystallogr.* **1999**, *32*, 837–838.

[18] C. T. Yang, B. Moubaraki, K. S. Murray, J. D. Ranford, J. J. Vittal, *Inorg. Chem.* **2001**, *40*, 5934–5941.

[19] K. Nakamoto, *Infrared and Raman Spectra of Inorganic and Coordination Compounds*, 5th ed., Wiley, New York, **1997**, p. 57.

[20] a) A. B. P. Lever, *Inorganic Electronic Spectroscopy*, Elsevier, Amsterdam, **1984**, p. 553; b) B. J. Hathaway, D. E. Billing, *Coord. Chem. Rev.* **1970**, *5*, 143–207.

[21] a) R. C. Holz, B. Bennett, G. Chen, L.-J. Ming, *J. Am. Chem. Soc.* **1998**, *120*, 6329–6335; b) N. N. Murthy, K. D. Karlin, I. Bertini, C. Luchinat, *J. Am. Chem. Soc.* **1997**, *119*, 2156–2162; c) J. M. Brink, R. A. Rose, R. C. Holz, *Inorg. Chem.* **1996**, *35*, 2878–2885; d) W. Kemp, *Organic Spectroscopy*, 3rd ed., Palgrave Publishers, New York, **1991**.

[22] a) V. H. Crawford, H. W. Richardson, J. R. Wasson, D. J. Hodgson, W. E. Hatfield, *Inorg. Chem.* **1976**, *15*, 2107–2110; b) F. Tuna, G. I. Pascu, J.-P. Sutter, M. Andruh, S. Golhen, J. Guillevic, H. Pritzkow, *Inorg. Chim. Acta* **2003**, *342*, 131–138; c) F. Tuna, L. Patron, Y. Journaux, M. Andruh, W. Plass, J.-C. Trombe, *J. Chem. Soc., Dalton Trans.* **1999**, 539–545.
[23] E. Ruiz, P. Alemany, S. Alvarez, J. Cano, *J. Am. Chem. Soc.* **1997**, *119*, 1297–1303.
[24] D. P. Kessissoglou, W. M. Butler, V. L. Pecoraro, *Inorg. Chem.* **1987**, *26*, 495–503.
[25] E. Gallo, E. Solari, N. Re, C. Floriani, A. Chiesi-Villa, C. Rizzoli, *J. Am. Chem. Soc.* **1997**, *119*, 5144–5154.
[26] D. Coucouvanis, K. Greiwe, A. Salifoglou, P. Challen, A. Simopoulos, A. Kostikas, *Inorg. Chem.* **1988**, *27*, 593–594.
[27] T. C. Higgs, K. Spartalian, C. J. O'Connor, B. F. Matzanke, C. J. Carrano, *Inorg. Chem.* **1998**, *37*, 2263–2272.
[28] O. Kahn, *Molecular Magnetism*, VCH Publishers, New York, **1993**, chapter 8.
[29] B. J. Hathaway, *Struct. Bonding (Berlin)* **1984**, *57*, 55–118.
[30] E. Garribba, G. Micera, *J. Chem. Educ.* **2006**, *83*, 1229–1232.
[31] J. Peisach, W. E. Blumberg, *Arch. Biochem. Biophys.* **1974**, *165*, 691–708.
[32] H. Yokoi, A. W. Addison, *Inorg. Chem.* **1977**, *16*, 1341–1349.
[33] K. Várnagy, I. Sóvágó, K. Agoston, Z. Likó, H. Süli-Vargha, D. Sanna, G. Micera, *J. Chem. Soc., Dalton Trans.* **1994**, 2939–2945.
[34] A. Abragam, B. Bleaney, *Electron Paramagnetic Resonance of Transition Ions*, Oxford University Press, London, **1970**.
[35] A. P. Golombek, M. P. Hendrich, *J. Magn. Reson.* **2003**, *165*, 33–48.
[36] S.-B. Yu, C.-P. Wang, E. P. Day, R. H. Holm, *Inorg. Chem.* **1991**, *30*, 4067–4074.
[37] A. Gelasco, M. L. Kirk, J. W. Kampf, V. L. Pecoraro, *Inorg. Chem.* **1997**, *36*, 1829–1837.
[38] a) S. Blanchard, G. Blondin, E. Rivière, M. Nierlich, J.-J. Girerd, *Inorg. Chem.* **2003**, *42*, 4568–4578; b) S. Blanchard, G. Blain, E. Rivière, M. Nierlich, G. Blondin, *Chem. Eur. J.* **2003**, *9*, 4260–4268.
[39] a) E. J. Laskowski, D. N. Hendrickson, *Inorg. Chem.* **1978**, *17*, 457–470; b) B. Mabad, P. Cassoux, J.-P. Tuchagues, D. N. Hendrickson, *Inorg. Chem.* **1986**, *25*, 1420–1431; c) H. Adams, N. A. Bailey, N. Debaeker, D. E. Fenton, W. Kanda, J.-M. Latour, H. Okawa, H. Sakiyama, *Angew. Chem. Int. Ed. Engl.* **1995**, *34*, 2535–2537; d) B. Albela, M. Corbella, J. Ribas, I. Castro, J. Sletten, H. Stoeckli-Evans, *Inorg. Chem.* **1998**, *37*, 788–798; e) T. Howard, J. Telser, V. J. DeRose, *Inorg. Chem.* **2000**, *39*, 3379–3385; f) I. Romero, M.-N. Collomb, A. Deronzier, A. Llobet, E. Perret, J. Pécaut, L. Le Pape, J.-M. Latour, *Eur. J. Inorg. Chem.* **2001**, 69–72.
[40] A. K. Whiting, Y. R. Boldt, M. P. Hendrich, L. P. Wackett, L. Que Jr., *Biochemistry* **1996**, *35*, 160–170.
[41] G. H. Reed, G. D. Markham, *Biological Magnetic Resonance* (Eds.: J. Reuben, L. J. Berliner), Plenum Press, New York, **1984**, p. 73–142.
[42] *WINEPR SimFonia*, version 1.25, Bruker Analytische Messtechnik GmbH, Karlsruhe, **1996**.
[43] *SMART and SAINT*, Bruker AXS Inc., Madison, Wisconsin, USA, **1997**.
[44] G. M. Sheldrick, *SADABS*, University of Göttingen, Germany, **1996**.
[45] G. M. Sheldrick, *SHELXL*-97, University of Göttingen, Germany, **1997**.
[46] B. V. Nonius, *NONIUS COLLECT, DENZO, SCALEPACK, SORTAV, Kappa CCD Program Package*, Delft, The Netherlands, **1999**.
[47] G. Cascarano, A. Altomare, C. Giacovazzo, A. Guagliardi, A. G. G. Moliterni, D. Siliqi, M. C. Burla, G. Polidori, M. Camalli, *Acta Crystallogr., Sect. A* **1996**, *52*, C-79.
[48] D. J. Watkin, C. K. Prout, J. R. Carruthers, P. W. Betteridge, *CRYSTALS*, Chemical Crystallography Laboratory, Oxford, United Kingdom, **1999**.
[49] A. D. Becke, *J. Chem. Phys.* **1993**, *98*, 5648–5652.
[50] M. J. Frisch, G. W. Trucks, H. B. Schlegel, G. E. Scuseria, M. A. Robb, J. R. Cheeseman, V. G. Zakrzewski, J. A. Montgomery, R. E. Stratmann, J. C. Burant, S. Dapprich, J. M. Millam, A. D. Daniels, K. N. Kudin, M. C. Strain, O. Farkas, J. Tomasi, V. Barone, M. Cossi, R. Cammi, B. Mennucci, C. Pomelli, C. Adamo, S. Clifford, J. Ochterski, G. A. Petersson, P. Y. Ayala, Q. Cui, K. Morokuma, D. K. Malick, A. D. Rabuck, K. Raghavachari, J. B. Foresman, J. Cioslowski, J. V. Ortiz, B. B. Stefanov, G. Liu, A. Liashenko, P. Piskorz, I. Komaromi, R. Gomperts, R. L. Martin, D. J. Fox, T. Keith, M. A. Al-Laham, C. Y. Peng, A. Nanayakkara, C. Gonzalez, M. Challacombe, P. M. W. Gill, B. G. Johnson, W. Chen, M. W. Wong, J. L. Andres, M. Head-Gordon, E. S. Replogle, J. A. Pople, *Gaussian 98* (Revision A.11), Gaussian, Inc., Pittsburgh, PA, **1998**.
[51] A. Schaefer, C. Huber, R. Ahlrichs, *J. Chem. Phys.* **1994**, *100*, 5829–5835.
[52] A. Schaefer, H. Horn, R. Ahlrichs, *J. Chem. Phys.* **1992**, *97*, 2571–2577.
[53] E. Ruiz, J. Cano, S. Alvarez, P. Alemany, *J. Comput. Chem.* **1999**, *20*, 1391–1400.

Received: February 25, 2009
Published Online: May 28, 2009

